RESEARCH PAPER

DIC-aided analysis of the fatigue behaviour of a welded 316L stainless steel

Amina Sriba[1] · Jérémie Bouquerel[2] · Jean-Bernard Vogt[2]

Abstract
The paper investigates the fatigue damage processes of a welded joint made of 316L stainless steel plates by using the digital image correlation (DIC) technique. First, the strain partition around a surface defect evidenced very high value of strain up to 10% at the notch root during the tension stage, which explained the poor fatigue life of some welded joint specimen. In healthy specimen, a strain gradient from the base metal to the fusion zone in the range of 0.3–0.6% to 3% respectively was evidenced. Fatigue crack always initiated in the fusion zone where the deformation concentrated either early in the fatigue life at high stress or progressively by a mechanism of deformation transfer from the base metal to the fusion zone at low stress.

Keywords Cracks · Image processing · Strain mapping · Defect · Welded joint

1 Introduction

Welding is one of the technologies employed to assembly components for making large structures. It is encountered as well in the transportation industries (automotive, aeronautics and railway equipment, etc.…) as in the energy production (nuclear, refineries…) and in the chemical engineering (acid production, polymer synthesis…). A welded joint consists of a fusion zone (FZ), heat-affected zones (HAZ) and the base metal (BM). The microstructural contrast created between these three zones makes the welded joint a hybrid material due to the variation in the material metallurgy. A welded joint is expected to exhibit at least the same performances as the base metal, but unlike the monolithic base metal, it may have different origins for its damage. Moreover, welded structures are more often subjected to variable and repeated loads of various origins (forces, pressure, thermal

expansions, centrifugation, etc.) during their working in industrial manufacturing. They can undergo large inelastic deformations which alter their metallurgical and mechanical characteristics, cause initiation and propagation of fatigue cracks. The fatigue phenomenon leads to the welded component failure. It is therefore crucial to assess the fatigue behaviour of the welded joints for safety and economic reasons. Each part in the welded joint contributes to the overall mechanical strength, and for that reason, their own mechanical behaviour needs to be identified.

The ball indentation [1] and the Small Punch Test (SPT) methods [2–10] are interesting measurement techniques that allowed estimation of monotonic mechanical properties such as yield stress or toughness because they require a few amount of material. This tends to make them very suitable for the assessment of the mechanical behaviour of the different parts of a welded joint. For instance, this has been successfully employed for creep [7]. However, they are semi destructive methods since it requires destroying the welded joint in order to extract lamella of material to be tested, and they are not in general well adapted for cyclic loading. Especially, the fatigue performance of materials, including welded material, is not limited to the fatigue life but also to the evolution of the mechanical properties during cycling, which is in general referred to cyclic accommodation. Since the metallurgical microstructure of each part of a welded joint is different, their cyclic accommodation can also be different, and this impacts the location of crack initiation. It is therefore of prime

---

✉ Jean-Bernard Vogt
jean-bernard.vogt@centralelille.fr

1 Research Centre in Industrial Technologies (CRTI), P.O. Box 64, 16014 Cheraga, Algiers, Algeria

2 Univ. Lille, CNRS, INRAE, Centrale Lille, UMR 8207 – UMET – Unité Matériaux Et Transformations, 59000 Lille, France

interest to determine the cyclic accommodation of each part of the welded joint. The use of several extensometers sensors attached at local parts of the welded joint specimen aimed at determining their individual behaviour, but the method is complex [11]. The cyclic ball indentation technique [12] answers such questions but does not allow pointing out if any interactions occurred between the different parts of the welded joint. The digital image correlation (DIC) technique has the particularity to acquire local displacement at the surface of a material in order, then, to map the strain field point by point in a wide surface area. DIC has the advantage to be a non-destructive method.

Advances in optical based techniques, regarding both hardware and software aspects, have greatly improved the DIC analytic options, and then, find many applications including local monotonic and cyclic plasticity measurement as well as crack detection [13–15]. The principle of DIC consists in collecting consecutive photos of the surface of an object before and during the deformation period. The collected digital images are analysed by a commercial or non-commercial DIC software to obtain a set of displacement maps for the entire specimen surface from which strain and/or stress fields can be calculated. DIC is widely used in determining the properties and mechanical performances of welded joints [16–18]. It was used to determine the local hardening curves [19, 20] and the stress concentration factor of each zone in the welded joint. The stiffness for each local zone can also be obtained in order to optimize the global stiffness of the welded joint [21]. DIC can provide similar values of mechanical properties of weld material as those obtained from micro samples [22]. A good agreement has been found between the stress–strain curve of the fusion zone of a 316H stainless steel welded joint obtained with micro tensile specimen and the stress–strain curve obtained by DIC [23]. Strain distribution for a steel plate welded joint obtained by DIC has been used to estimate the low cycle fatigue life showing the versatility of this technique [24]. The influence of the butt weld seam geometry of welded joint made of AISI 347 and the microstructural inhomogeneities on the fatigue behaviour has been revealed with DIC [25].

The paper is focused on the low cycle fatigue of 316L plates welded with the gas tungsten arc welding (GTAW) process. 316L stainless steels are intended for applications where corrosion resistance is required and selected also thanks to their good mechanical properties (good strength, creep resistance and excellent mechanical at low temperature). This makes them applicable for a very wide range of applications, and the understanding of their mechanical

damage guarantees their reliability. However, in a test program of the assessment on the low cycle fatigue response of 316L welded joints, a large scattering was observed in the stress response to strain cycling as well as in the fatigue lives.

The objective of the paper is to identify in a non-destructive way the individual cyclic behaviour of the different parts of the welded joint submitted to fatigue tests. It aims at revealing qualitatively and quantitatively the deformation localization in the welded joint resulting from cyclic loading by the digital image correlation (DIC) technique. Coupling these DIC data with the identification of cyclic plasticity marks revealed by advanced SEM investigation, the different causes in the plastic deformation partition of the different constituents of the welded joint and their interaction will be discussed.

2 Material

The welded joint considered in this study material consists of 4-mm-thick 316L austenitic stainless steel plates as base metal welded using the GTAW process in the flat position and by employing the ER316LN stainless steel as filler material. The welded joint has been made in three passes with a shielding gas constituted of a mixture of argon (~ 96%) and hydrogen (~ 4%) and a flow rate of 11L/min. The chemical composition of the base metal and of the fusion zone of the weld joint after welding is reported in Table 1.

No heat treatment was performed on the base metal before welding or on the welded joint after welding.

Figure 1 shows the micrograph of the welded joint where both the base metal and the fusion zone are imaged. The base metal exhibits the classical equiaxed grain structure with a grain size of about 50 μm and contained approximately 4% of delta ferrite. The fusion zone is typical of a solidified structure with presence of dendrites. Near to the fusion zone, the base metal exhibits a band of about 200 μm wide of larger grain size as it corresponds to the heat-affected zone.

The heat-affected zone has the lowest hardness (145 HV ± 5) while the fusion zone was the hardest one (191 HV ± 5) and the base metal had a hardness value of 170 HV ± 5. Charpy tests have shown that the base metal and the welded joint had nearly the same impact energy (55 J) with for both a ductile fracture [26].

Table 1 Chemical composition (wt. %) of the base metal and the fusion zone of the welded joint 316L/ER316LN

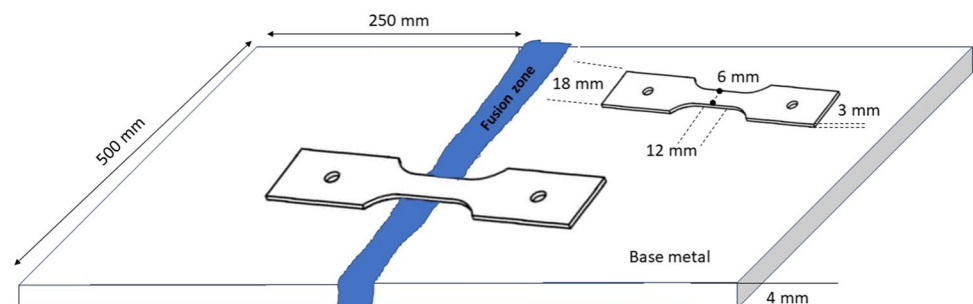| Material	C	Si	Mn	P	S	Cr	Mo	N	Ni	Cu	Fe
Base metal	0.025	0.367	0.988	0.031	‹ 0.0005	16.6	1.99	0.0595	10.6	0.46	Rest
Fusion zone	0.022	0.492	1.355	0.029	0.013	16.57	2.34	0.0400	9.41	0.52	Rest
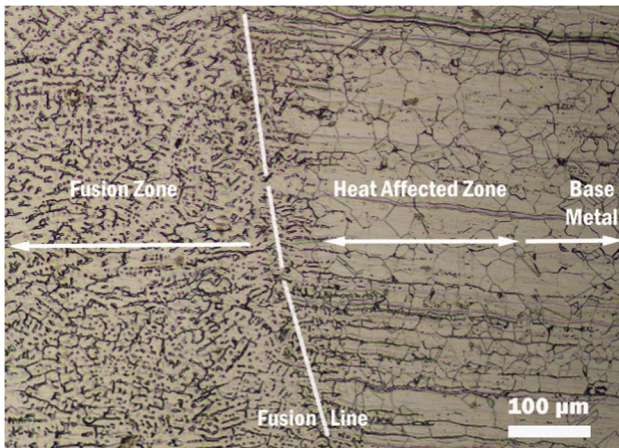
Fig. 1 Optical micrograph of the welded joint showing the base metal on the right side and part of the fusion zone on the left side

3 Experimental

3.1 General methodology

Fatigue tests can be carried out either under load (or stress) control or under strain control. When cycling conditions involve cyclic plasticity, a tested material can exhibit either softening or either hardening which is reflected differently according to the conducted type of fatigue test. If hardening occurs, then the stress values increase with the number of cycles under strain-controlled tests, and the strain values decrease during the stress-controlled test, before a stabilized state. The softening behaviour is associated with a stress decrease with the number of cycles in the strain-controlled test and a strain increase in the stress-controlled test which can reach very high values. Sometimes, these values are so high that they do not reflect progressive damage by fatigue. It is therefore of prime interest to perform strain-controlled test to appreciate the cyclic behaviour. It can be considered that for a material monolithic at the grain scale, the plastic deformation is roughly homogenously distributed in the fatigue specimen. In the case of a hybrid material such as a welded specimen, the deformation is different in each part of the weld because of their differences in individual mechanical strength (hardness, yield stress). It turns out doing a fatigue test under total strain control by using an extensometer measuring the displacement between two points widely spaced and comprising different parts of material is not relevant. Indeed, the individual deformation of each part of the material is not the same, and the cyclic accommodation of each part cannot be identified since the recorded stress response is the macroscopic total one resulting from the sum of the different individual ones.

Therefore, we have decided to conduct two sets of fatigue tests. The first one is strain-controlled tests to identify the cyclic accommodation of the monolithic base metal and of the welded material. The second one is load-controlled tests with the purpose of assessing the individual behaviour of each part of the welded specimen. The parameters of this second set of tests will be inferred from the strain-controlled tests. For both sets of fatigue tests, plate fatigue specimens were machined from the plates of the 316L base material and from the welded plates. Specimens had a thickness of 3 mm, a width of 6 mm and a gage length of 12 mm. For the welded materials, the machining was performed so that the gage part contained both the base metal and the fusion zone, the latter being in the middle of the specimen as shown in Fig. 2.

Before testing, each specimen was mechanically polished on both sides in order to remove the work-hardened surface due to the machining step. A mirror-like surface was obtained by using successively silicon carbide paper from grade 80 to grade 1200, and then diamond suspensions 6 μm, 3 μm and 1 μm.

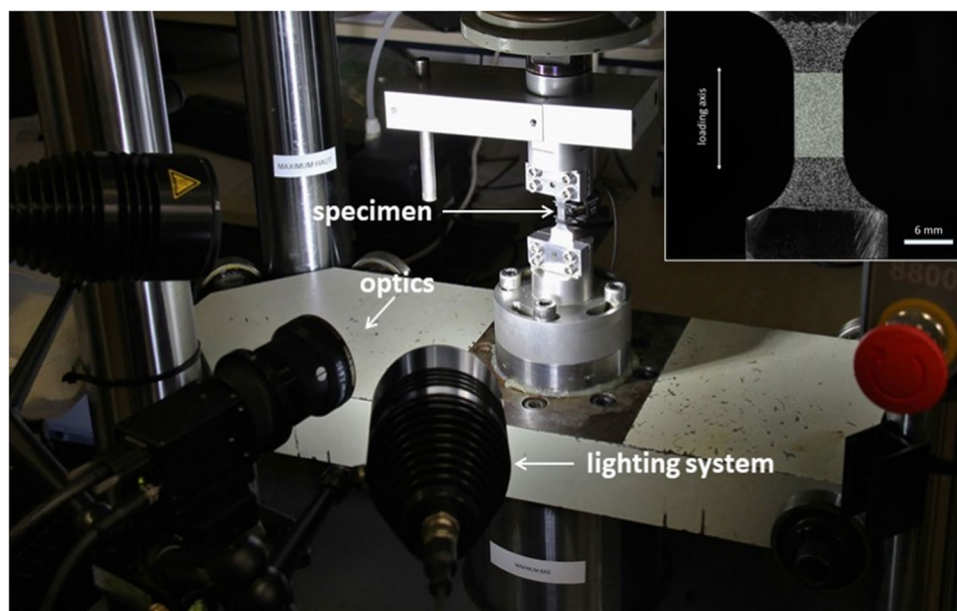### 3.2 Procedure for assessment of stress response to strain cycling

Low cycle fatigue (LCF) experiments were conducted on the monolithic 316L base metal as well as on the welded joint fatigue specimen at room temperature in air. The fatigue tests were carried on an electromechanical Schenck Trebel RMC100 fatigue machine with a load capacity of 50 kN using an Instron 8800 mini-controller. Tests were performed up to failure under total axial strain control $\Delta\varepsilon_t = 0.6\%$, 0.8%

Fig. 2 Sampling location in the fabricated welded plate and specimen dimension for characterisation of the welded material and of the base metal

and 1% by using a 10 mm gage extensometer. A fully push pull mode (strain ratio $R_\varepsilon = -1$), a triangular waveform and a constant strain rate of 4.10^{-3} s^{-1} were used.

3.3 Procedure for strain assessment with fatigue-DIC tests of the different zones of the welded material to stress cycling

Fatigue-DIC tests were conducted only on the welded joint specimen under load control in fully push pull mode by using a triangular waveform, at room temperature in air, with the same fatigue machine mentioned above. Tests were performed under load control $\Delta F = 6.8$ kN, $\Delta F = 8.4$ kN and $\Delta F = 10$ kN, with a load ratio $R_F = -1$ and a frequency of 0.25 Hz. These values were selected after having done the strain-controlled tests. Specimen had also the same shape as for LCF experiments but was prepared for DIC analyses. For that, the specimens were first mechanically polished up to 3 μm. Then, to obtain a speckle surface, a white antireflection paint was applied uniformly on the surface. Once it was dried, a graphite-based spray was applied in order to obtain a correct grey distribution from the random repartition of black dots on the surface. The sample was then put into the fatigue testing machine, and the camera was placed in front of the specimen at 90° to its surface. DIC was performed with Aramis application system including a CCD camera (Fig. 3) and Aramis v6.3 software developed by GOM Company. The camera, equipped with a 100 mm lens, has a resolution of 2448×2050 pixels and a maximum frame rate of 15 Hz. Each DIC image of the specimen gage part covers a frame of 6 mm $\times$ 12 mm composed of 400×800 pixels resulting in a spatial resolution of 276 μm with the setting parameters of the system.

4 Results and discussion

4.1 LCF behaviour

The stress response to strain cycling of the 316L base metal and of the welded joint is shown in Fig. 4a and b respectively. The 316L base metal exhibits a cyclic hardening followed by a cyclic softening and then a quasi-stabilization of the stress. The duration of the hardening stage and the intensity of the hardening increases with the increase of the applied strain variation.

By contrast, the softening period is all shorter that the strain variation is high. The strong decrease in the stress at the end of the test is associated with the propagation of a long crack in the bulk. The welded joint also hardens at the beginning of the fatigue life but then continuously softens up to failure without any stabilization occurring.

A high scattering of the data has been observed for the tests on the welded joint specimen. In particular, considering a given strain range, the stress amplitude values as well the fatigue life can be very different from one test to another. In terms of fatigue resistance, in average, there was not so big difference between the base metal specimens and the welded joint specimens except for some welded joint specimens which failed very early because of a pre-existing welding defect. This will be further commented.

The literature results on the fatigue behaviour of 316 L stainless steel including the cyclic accommodation and the fatigue life show that some variations can be observed from one grade to another. This is the result of the initial microstructure before the cycling of the material.
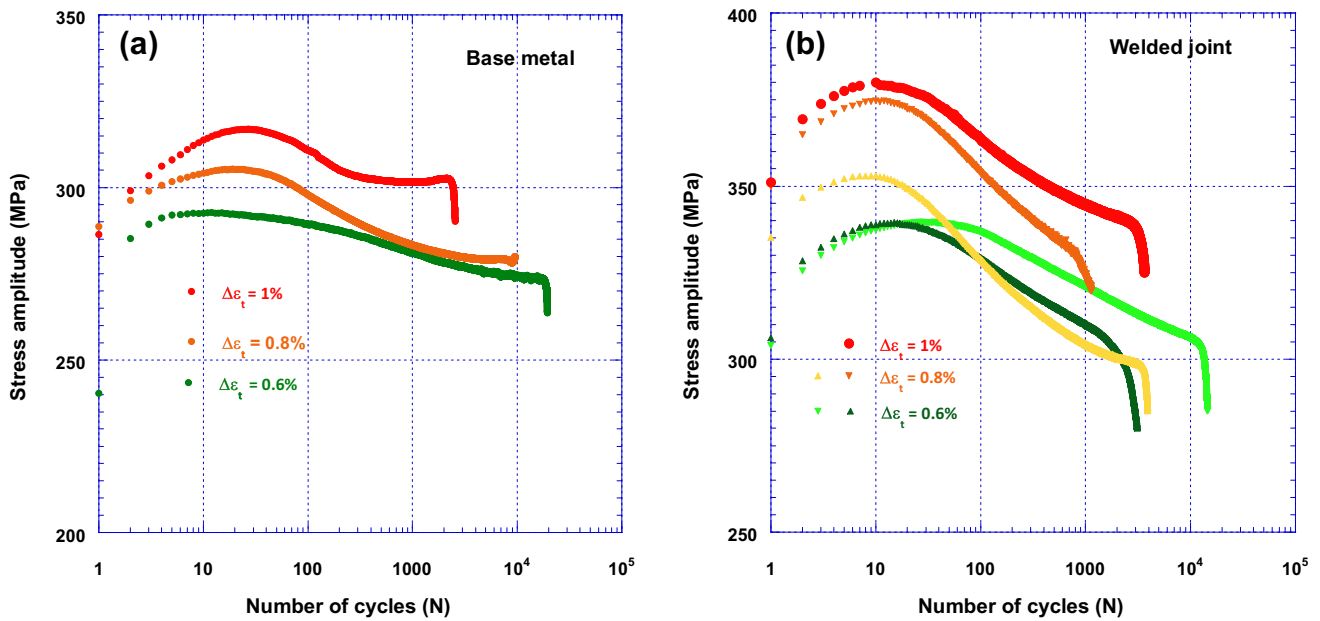

Fig. 3 Experimental setup of fatigue-DIC tests; the embedded image shows the field of view of the camera

Fig. 4 Evolution of the stress amplitude with the number of cycles for the base metal (**a**) and for the welded joint (**b**)

Cold-worked 316L obviously tends to strongly soften during cycling [27]. The chemical composition especially nitrogen has an impact not only on the stress values as a result of solid solution hardening but also on dislocation slip mode and austenite stability [28, 29]. This is why it was first necessary to perform a restricted number of tests on the 316L base metal before investigating the fatigue behaviour of the 316L welded steel. The results obtained in the present study are consistent with most of the published results. Especially, they fit well with those published by Agrawal et al. [30] or Samir Chandra Roy et al. [31] in terms of stress response to strain cycling, stress value and fatigue lives. The initial hardening followed by a softening and quasi stable cyclic stress suggests that the dislocations involved in the cyclic accommodation have arranged into a rather stable arrangement. Veins/channels and walls/channels are classically observed in this range of

applied strains, and planar arrangements are promoted by decreasing strain amplitude while increasing strain amplitude results in denser dislocation walls and cells [32–34].

4.2 Slip marks and crack initiation

At the end of the tests, the fatigue specimens of the 316L base metal were covered by intrusions-extrusions as shown in Fig. 5a from where short cracks initiated. The density of slip marking increased with the applied strain range.

After fatigue failure, the welded joint specimens were also covered by slip marks in the form of extrusions (Fig. 5b), both in the base metal and in the fusion zone. The extrusions are however longer in the fusion zone in regard to the microstructure which contains wider areas for plastic deformation.

Fig. 5 Fatigue extrusions after fatigue test at $\Delta\varepsilon_t = 1\%$ in the base metal (**a**) and after fatigue test at $\Delta\varepsilon_t = 0.8\%$ for the welded joint (**b**)
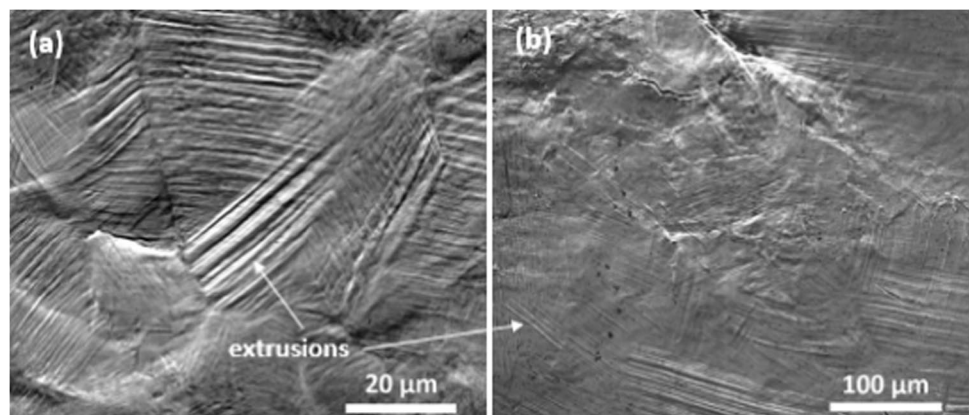
Crack initiated and propagated in the fusion zone of the welded joint (Fig. 6) even if for the low strain test the density of extrusions was not as high as in the base metal. Fatigue fracture in the fusion zone of a 316LN austenitic stainless steel welded joint has also been reported by Chandra et al. [35] and Jiang [36] after LCF test at high strain range.

4.3 Strain assessment with load-controlled fatigue-DIC tests of the welded joint

Different tests were conducted at a load variation $\Delta F = 6.8$ kN, $\Delta F = 8.4$ kN and $\Delta F = 10$ kN. Assuming that the initial cross section of the specimen does not change so much during cycling, the load variations correspond to stress variations $\Delta\sigma = 378$ MPa, $\Delta\sigma = 466$ MPa and $\Delta\sigma = 555$ MPa respectively. In agreement with the strain-controlled fatigue tests performed on the welded specimen, a strong scattering in the fatigue lives was observed, which incited to treat the data according to the quality of the weldment. Indeed, the presence of a weld defect in a welded joint can cause a severe stress concentration around that area which results in a detrimental effect on fatigue crack initiation [37–39]. However, the effect of a weld defect as well as any defect will produce an effect according to its shape, sizes and loading conditions. In the test package of the present paper, our specimen contained either obvious weld defects such as those visible at the external surface of the specimen or nonvisible being inside the bulk of the specimen. For the latter, some of them had an impact on the fatigue life while the other ones were probably too few or too small to affect the fatigue response. Their evidence depends on the resolution of the non-destructive technique if employed. In the following, the welded joints will be considered as healthy welded joints when the fusion zone is free of defects or when it contains harmless defects because of their size and quantity. Otherwise, they will be classified as defective welded joints. In the following, only the highest normal strain will be reported in the strain mapping since this component helps the opening of the crack. Moreover, the shear strain was also estimated additionally but was very small compared to the normal strain.
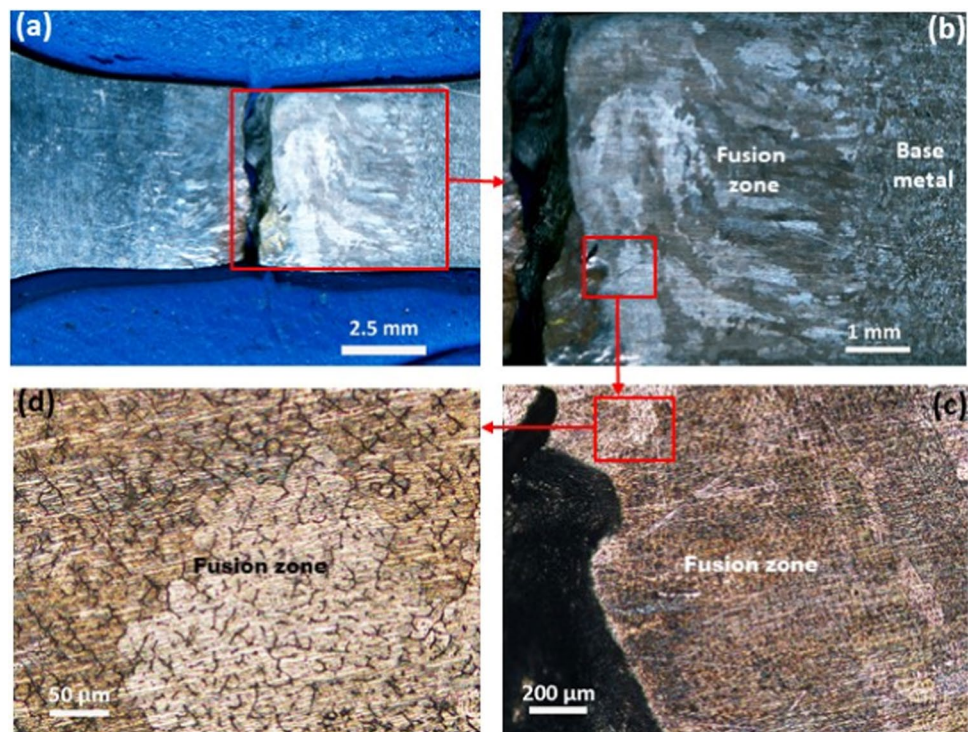
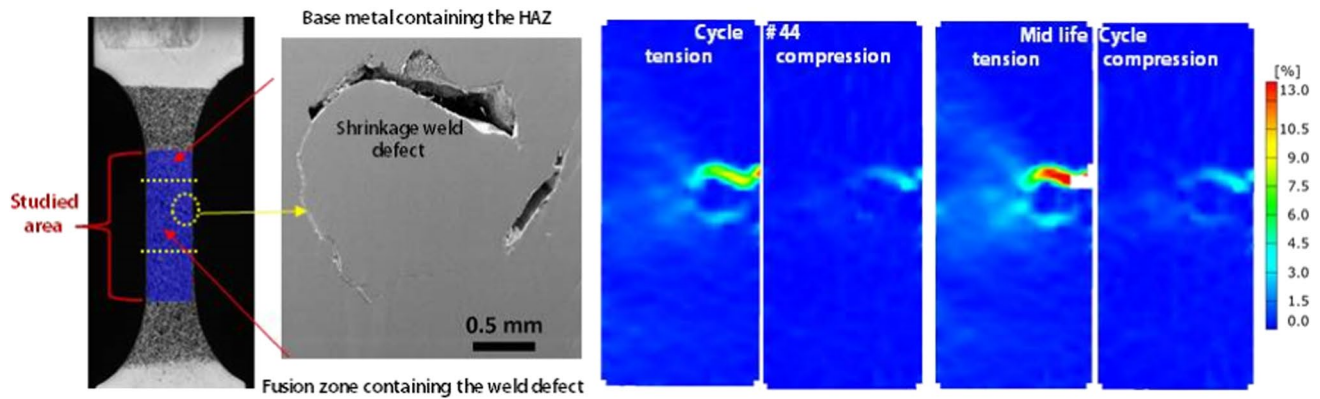### 4.3.1 Defective welded joint containing visible defects

In these defective welded specimens, the presence of the defect was very obvious since it appeared at the external surface and could be suspected sometime, if deep attention was paid, with the naked eye. In this paragraph, the test performed at a load $\Delta F = 6.8$ kN is shown. The fatigue life was 1021 cycles instead of 6565 cycles for the free defect specimen.

The strain mapping shown in Fig. 7 suggests that the fusion seems to be inactive on the whole except near the defect where stress concentration developed.

The deformation concentrates at a local spot since the very first cycles of fatigue in the fusion zone while the base metal is inactive. It is important to note that the strain

Fig. 6 Optical macrographs (**a**, **b**) and optical micrographs (**c**, **d**), showing the location of the fracture in the fusion zone of the welded joint at various magnifications after fatigue test at $\Delta F = 8.4$ kN

Fig. 7 Strain mapping recorded at different numbers of cycles during fatigue test at $\Delta F = 6.8$ kN at the surface of welded joint fatigue specimen containing a visible weld defect

reached a very high value up to 10% near the defect. During the compression phase, the strain localisation vanishes.

4.3.2 Defective welded joint containing invisible defects

In these defective welded specimens, the defect was an inclusion whose presence and possible effect could be pointed out once the test has been started and after DIC analysis and fractographic observations. The specimen was cycled at a load $\Delta F = 10$ kN and failed after 206 cycles while a healthy weld joint failed after 1276 cycles. The strain mapping (see Fig. 8) shows that the deformation was again concentrated inhomogeneously in the fusion zone very early in the fatigue life. It can be seen a small, sharp and highly strained area from which intensive inclined bands of deformations develop. Increasing the number of cycles tends to increase the strain at any point of the deformed zone in the tension phase of the fatigue test. During the compression, the average strain is strongly reduced, but the localisation of the deformation is still visible. Finally, fatigue crack initiates at the highly deformed site and propagate in the fusion zone. After fatigue failure into two parts of the specimen, the fracture surface was observed, and strain localisation associated to fatigue crack initiation was attributed to the presence of two inclusions.

4.3.3 Strain assessment in a healthy welded joint

The strain mapping for different numbers of cycles in a healthy welded joint is reported in Figs. 9 and 10 for the test performed at $\Delta F = 10$ kN and $\Delta F = 8.4$ kN respectively. The tests performed at $\Delta F = 6.8$ kN and $\Delta F = 8.4$ kN gave a similar response.

For the highest load test (Fig. 9), when the welded joint was submitted to the first loading, the deformation mainly localizes in the middle of the specimen. The deformation concentrates in the fusion zone in a very narrow area since the first cycles of fatigue. This area exhibits an inhomogeneous partition of the strain which increases with the number of cycles, and the highly strained zone expands towards the base metal. There exists a strain gradient from the fusion zone to the base metal.

For the two lowest load conditions, the situation contrasts with the previous one. Indeed, highly localized deformation in the fusion zone is not observed at the beginning of the test. The strain slightly increases at the beginning of cycles and remains rather stable for a large part of the fatigue in localized zones which correspond to the heat-affected zone of the base metal (Fig. 10).

By considering the evolution of the strain during the compression and the tension phases, this situation lasts for about 1950 cycles even though there exists a dissymmetry between tension and compression. Then, at around 1950 cycles, the highest strained zone turns to the middle part of the specimen, i.e. the fusion zone where crack initiation takes place (Fig. 11).

The activity of plastic deformation was also pointed out with the observations of dislocation arrangements. For that, the electron channelling contrast imaging technique (ECCI) was employed because it allowed observations of dislocations by SEM of dedicated zones without cutting the specimen. Figure 12a shows that the grains of the fusion zone contain a high density of dislocation planes. In contrast to the base metal which developed well-formed dislocation configurations (cells, walls), see Fig. 12b, such arrangements were not found in the fusion zone, and dislocations were displayed within the slip planes.

5 Discussion

The present work focused on the low cycle fatigue behaviour of 316L stainless steel welded joint revealing a clear difference with that of the 316L base metal. Indeed, both
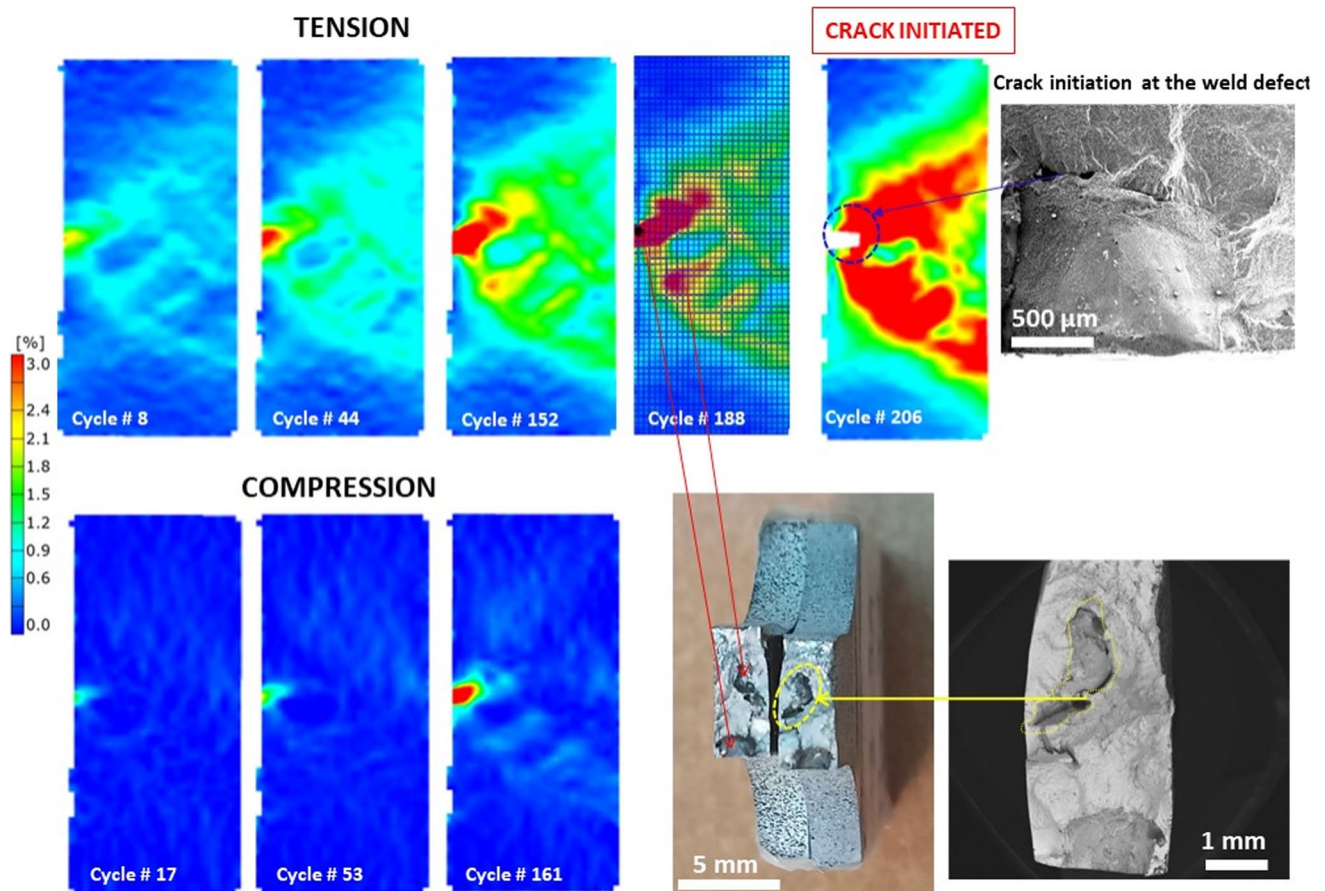
Fig. 8 Strain mapping recorded at different numbers of cycles during fatigue at $\Delta F = 10$ kN at the surface of welded joint fatigue specimen free of visible defect and fracture surface showing inclusion cavity

Fig. 9 Strain mapping recorded at different numbers of cycles during fatigue in the tension phase at $\Delta F = 10$ kN at the surface of welded joint healthy fatigue specimen
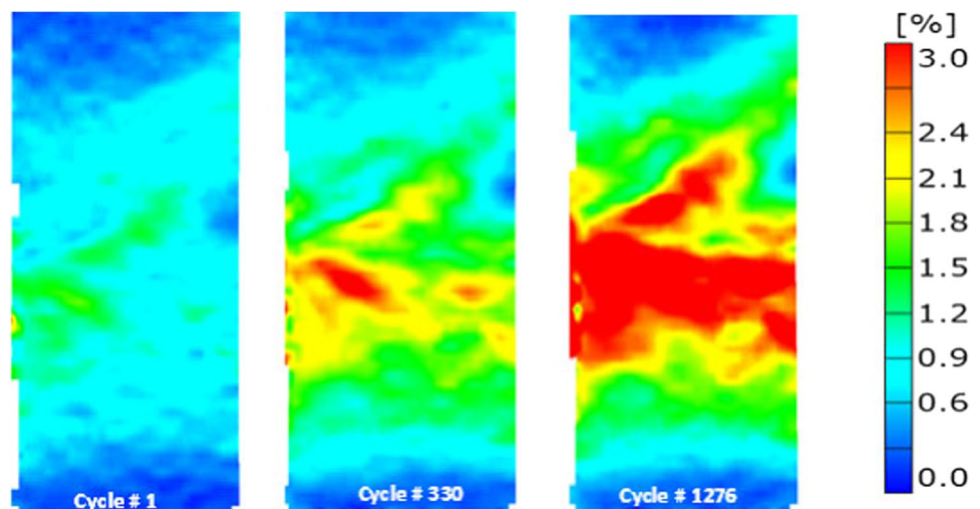

the stress response to strain cycling and the fatigue resistance of the welded joint could not be simply inferred from the behaviour of the base metal. This led us to consider two groups of welded joint specimens, one with healthy welded joints and another with defective welded joints. The study has showed the high potentiality of the DIC technique for clarifying the specific fatigue response of the welded material. At first, DIC has been used in the most conventional

Fig. 10 Strain mapping recorded at different numbers of cycles during fatigue at $\Delta F = 8.4$ kN at the surface of a welded joint healthy fatigue specimen
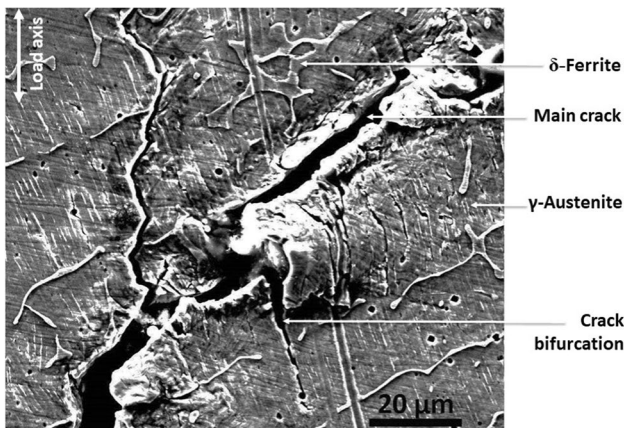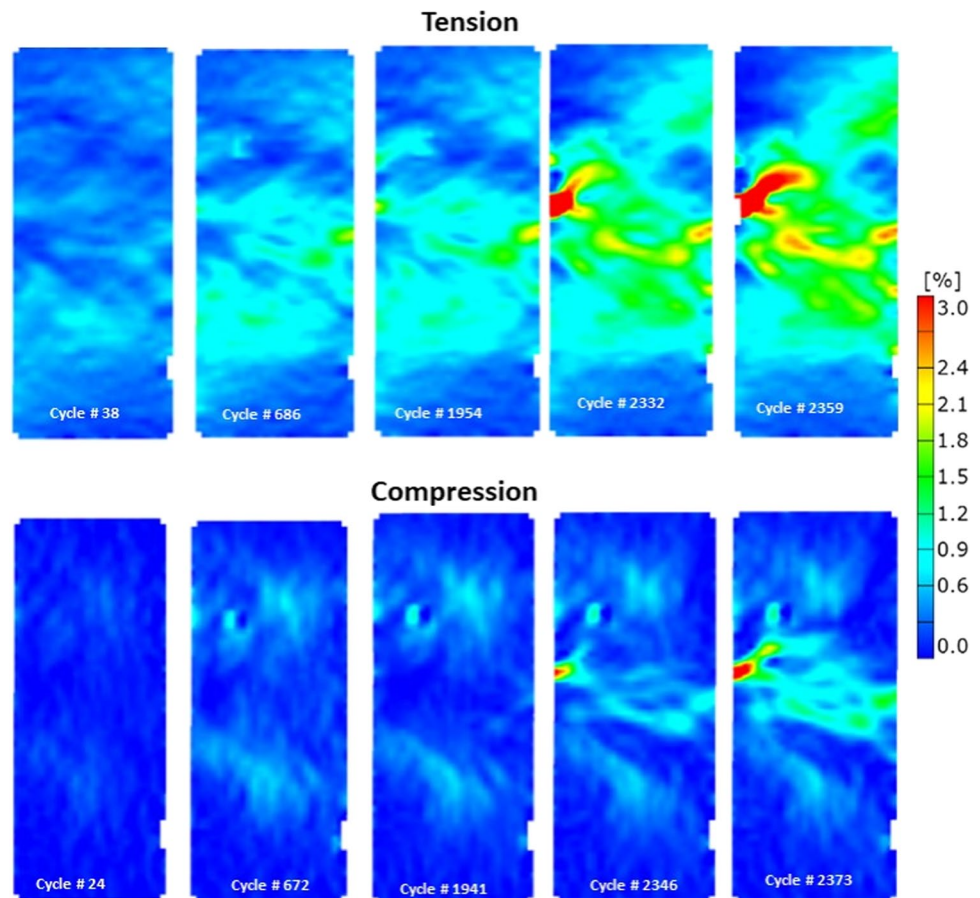
**Fig. 11** Main fatigue crack located in the fusion zone of the welded joint after failure

way, i.e. the collection of displacement fields of the fatigue specimen which is the basis for strain and/or stress calculations in order to identify the local mechanical hot spots of the material. But more striking, our study shows that DIC can also answer and solve questions related to damage and cyclic plasticity mechanism which are discussed below.

5.1 Defective welded joints

In the group of specimens with a defective welded joint, the defects were identified either as solidification shrinkage (Fig. 7) or as inclusion (Fig. 8). Solidification shrinkage results from the transformation of liquid to solid and may grow as it cools to room temperature due to additional thermal contraction. It can appear at the surface, and it can be located in the bulk of the material and therefore invisible from the outside. The resulting detrimental effect of this defect present at the external surface is the most classical and expected one since it provides stress concentration at the notch root. One of the interesting inputs of DIC in this case is the highlight of the very high and local strain — more than 10% — reached at the defect root (Fig. 7). It also evidences the detrimental presence of the defect during the opening phase of the loading.

Inclusions, even if they do not appear as a lack of material, need also to be considered. They are known to play an important role in many mechanical and corrosion properties of metallic alloys. For steels, in general, non-metallic inclusions are hard and less deformable than the matrix in which they have been confined during solidification. In very high cycle fatigue, inclusions are the sites of crack initiated in the

Fig. 12 SEM ECCI images showing (**a**) individual dislocations spread in the austenitic phase of the fusion zone and (**b**) dipolar walls in the austenitic base of the welded joint cycled under $\Delta F = 8.4$ kN
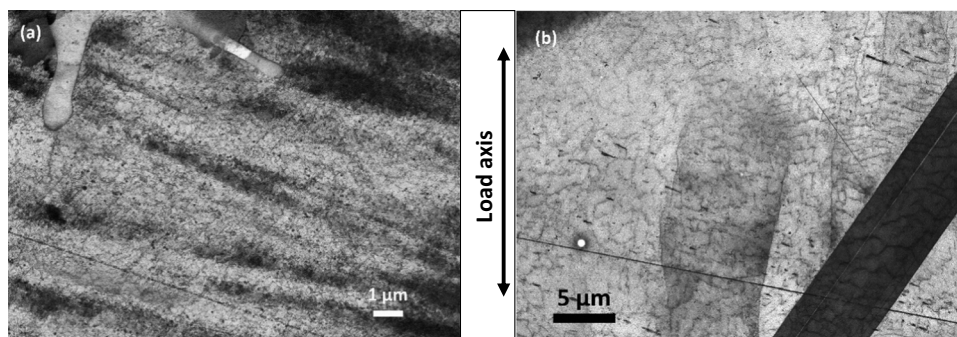
sub-surface [40]. The nature, the size and the distribution are the main parameters that will affect the fatigue resistance. In the present investigation, the inclusion embedded inside the fusion zone, not visible from outside (Fig. 8), was assigned to tungsten weld contamination possibly caused by the tungsten electrode fusion or its contact with the bath fusion during welding operation. The results pointed out an additional cause of local deformation due to the presence of an inclusion located under the surface. The advantage of the DIC technique was to identify the possible site of crack nucleation. In addition, it points out the harmful effect of the inclusion during the tensile phase of the loading. Indeed, there is a big difference between the strain value calculated during the tension phase and the compression phase and also the expanse of the deformation zone. It is interesting to note that such an inclusion can highly deform the surrounding matrix very early in the fatigue life of the material.

5.2 Healthy welded joints

Compared to defective welded joints, in healthy welded joints, the cyclic loading did not result to very large localized strain very early thanks to the absence of a pre-existing defect or cracks. In these specimens, a large part of the fatigue test is to initiate a fatigue crack which comes from the gliding of dislocations in each part of the welded joint.

The DIC strain mapping showed that the response of the welded joint was load dependent which can be explained by the typical cyclic strain accommodation of each part of the welded joint. Indeed, the fusion zone (FZ) and the heat-affected zone (HAZ) which represents the main part of the gage length of the welded joint specimen had differences in hardness values [26]; both of them contribute in the deformation of the gage length but not with the same magnitude. This is proved by the network of slip markings well developed in both parts of the welded joint specimen, which clearly indicates that both were very active in the accommodation of the cyclic deformation (Figs. 5 and 12). 316L austenitic stainless steel is featuring cyclic softening, as depicted with the low strain-controlled test, which results from a rate of dislocation annihilation likely higher than the

rate of production. From the strain-controlled tests and considering a given strain range, the cyclic stress values higher for the welded joint specimen than for the monolithic base metal specimen recorded during cycling (Fig. 4), especially during the cyclic hardening period, originate from the fusion zone, which is harder than the HAZ and the base metal [26]. But the more intense softening in the case of welded joint specimen may a priori result from the softening of the HAZ or of the fusion zone or of both zones. A cyclic softening behaviour of the fusion zone has been directly pointed out with fatigue experiments on specimen taken from the weld metal of a 316L(N)/316L(N) welded joint [41] but not clearly proved.

The results of the present paper show that when the applied load is low, the base metal is the first part of the weld to react, to soften and to become progressively less and less able to accommodate the plastic deformation. As a result, the deformation accommodation is transferred to the other part of the weld, i.e. the fusion zone. Such a deformation transfer process has already been suggested explaining the cyclic plasticity of a duplex stainless steel for which one of the phases compensated the vanishing action of the other one in the accommodation of the plastic deformation [42, 43]. Once the deformation is transferred to the fusion zone, the latter now accommodates the plastic deformation. The increasing strain values in the fusion zone clearly indicate that the latter is now cyclically softening. The DIC strain mapping also indicates that once the deformation was transferred from the base metal to the fusion zone, the latter was the site for an early crack initiation and for crack propagation leading to the failure of the specimen. This means that the more the base metal exhibits softening, the more rapid is the deformation transfer from the base metal to the fusion zone. This is a crucial point for the corrosion-fatigue resistance in situations where the fusion zone is protecting the base metal. The control of the cyclic softening in 316L stainless steel MIG-welded joints by thermal and mechanical treatment has been investigated by Guizani et al. [44]. For a low strain test, the mechanical brushing treatment allowed reducing the cyclic softening which resulted in longer fatigue life. Crack initiation in the fusion zone of a welded material with

bainitic steel as base metal has been reported by K. Xu et al. [45]. These authors assumed the origin of crack initiation in the fusion zone as a consequence of its cyclic softening. However, the use of DIC in our investigation clearly demonstrates that the cyclic accommodation of the welded joint specimen results from an interaction between the base metal and the fusion zone and not from their individual responses, which constitutes an innovative outcome in the understanding of the cyclic deformation at low load of welded joints made of 316 stainless steel. By using these strain-controlled fatigue tests, the local strain measurement would have been impracticable but the stress control coupled to DIC allows clarifying these questions.

For the high load test ($\Delta F = 10$ kN) where both the fusion zone and the base metal deformed since the very first cycles (Fig. 9), there is no interaction between them and each cyclically deformed according to their own cyclic work hardening rate. The increasing strain in the fusion zone also suggests that the material becomes softer and softer as a result of the strong cyclic softening property that exhibits the fusion zone. Crack initiation takes place in this zone before any occurrence of deformation transfer towards the base metal.

6 Conclusion

The fatigue behaviour of a 316L stainless steel welded joint and of the 316L stainless steel base metal has been investigated. The DIC technique has been employed in order to point out the stress raiser effect due to visible and non-visible welding defects. Moreover, using load-controlled tests with DIC, the interactive response of each part of the welded joint has been pointed out. The main conclusions derived from this work are as follows:

1. Both the base metal and the welded joint exhibited initial cyclic hardening followed by cyclic softening which was more pronounced for the welded joint than the base metal. Also, the stress level was higher for the welded joint
2. There was a high scattering in the fatigue results for the welded joint attributed to the presence of welding defects which provide large strain up to 10% localized at the defect root
3. The DIC technique obviously revealed high strain values near a defect but appeared able to evidence the strain concentration of non-visible defects
4. The strain mappings performed on healthy welded joints showed that there is a critical stress above which the behaviour of the welded joint is controlled by the fusion zone alone while below it is controlled first by the base metal for a long part of the fatigue life and then later on by the fusion zone.

5. At low cyclic stress, the cyclic softening observed on the welded joint is associated with the deformation transfer mechanism from the base metal to the fusion zone
6. Fatigue cracking was always observed in the fusion zone where strain could reach values up to 3% while the base metal remained less deformed (0.3–0.6%), which suggests that its own fatigue resistance should control the fatigue life of the welded joint

Declarations

Ethics approval The authors declare that the results have not yet been published elsewhere.

Conflict of interest The authors declare no competing interests.

References

1. Sharma K, Khandelwal HK, Bhasin V, Chhibber R (2012) Application of ball indentation technique for mechanical properties estimation of bi-metallic weld. Adv Mater Res 585:342–346. https://doi.org/10.4028/www.scientific.net/AMR.585.342
2. Abendroth M, Soltysiak S (2016) Assessment of material properties by means of the small punch tesT. Recent Trends in Fracture and Damage Mechanics 127–157. https://doi.org/10.1007/978-3-319-21467-2_6
3. Abendroth M, Kuna M (2004) Determination of ductile material properties by means of the small punch test and neural networks. Adv Eng Mater 6(7):536–540. https://doi.org/10.1002/adem.200400405
4. Auger T, Serre I, Lorang G, Hamouche Z, Gorse D, Vogt JB (2008) Role of oxidation on LME of T91 steel studied by small punch test. J Nucl Mater 376:336–340. https://doi.org/10.1016/j.jnucmat.2008.02.076
5. Lyu DY, You HS, Yoon JY et al (1992) Fracture strength evaluation of welded steel joint by means of small punch test. KSME Journal 6:73–80. https://doi.org/10.1007/BF02953073
6. Altstadt E, Ge HE, Kuksenko V, Serrano M, Houska M, Lasan M, Bruchhausen M, Lapetite JM, Dai Y (2016) Critical evaluation of the small punch test as a screening procedure for mechanical

properties. J. Nucl Mater 472:186–195. https://doi.org/10.1016/j.jnucmat.2015.07.029

7. Li Y, Šturm R (2016) Punch test for weld heat affected zones. Mater High Temp 23:225–232. https://doi.org/10.1179/mht.2006.019

8. Fleury E, Ha JS (1998) Small punch tests to estimate the mechanical properties of steels for steam power plant: I. Mechanical strength. Int J Pres Ves Pip 75:699–706. https://doi.org/10.1016/S0308-0161(98)00074-X

9. Wen C, Xu T, Guan K (2016) Correlation factor study of small punch creep test and its life prediction. Mater 9(10):796. https://doi.org/10.3390/ma9100796

10. Roger Hurst C, Robert Lancaster J, Spencer Jeffs P, Martin Bache R (2016) The contribution of small punch testing towards the development of materials for aero-engine applications. Theor Appl Fract Mech 86:69–77. https://doi.org/10.1016/j.tafmec.2016.07.013

11. Mongabure P, Matheron P, Madi Y (2003) Mechanical cyclic behaviour of 316L welded joint. Mech Ind EDP Sciences 4:619–626. https://doi.org/10.1016/j.mecind.2003.09.003

12. Prakash RV, Madhavan K, Prakash AR, Sandhya R, Reddy GVP (2018) Fatigue response evaluation of stainless steel SS 304 L(N) and SS 316 L(N) through cyclic ball indentation studies. Ubiquity Proceedings 1(S1):38. https://doi.org/10.5334/uproc.38

13. Hutt T, Cawley P (2009) Feasibility of digital image correlation for detection of cracks at fastener holes. NDT and E Int 42:141–149. https://doi.org/10.1016/j.ndteint.2008.10.008

14. Corigliano P, Epasto G, Guglielmino E, Risitano G (2017) Fatigue analysis of marine welded joints by means of DIC and IR images during static and fatigue tests. Eng Fract Mech 183:26–38. https://doi.org/10.1016/j.engfracmech.2017.06.012

15. Górszczyk J, Malicki K, Zych T (2019) Application of digital image correlation (DIC) method for road material testing. Mater 12(15):2349. https://doi.org/10.3390/ma12152349

16. Reynolds AP, Duvall F (1999) Digital image correlation for determination of weld and base metal constitutive behaviour. Weld. Res. Suppl 355-360. https://doi.org/10.1007/s11340-006-9824-8

17. Saranath KM, Sharma A, Ramji M (2014) Zone wise local characterization of welds using digital image correlation technique. Opt and Lasers Eng 63:30–42. https://doi.org/10.1016/j.optlaseng.2014.06.006

18. Sierra G, Wattrisse B, Bordreuil C (2008) Structural analysis of steel to aluminum welded overlap joint by digital image correlation. Exp. Mech 48:213–223. https://doi.org/10.1007/s11340-007-9112-2

19. Genevois C, Deschamps A, Vacher P (2006) Comparative study on local and global mechanical properties of 2024 T351, 2024 T6 and 5251 O friction stir welds. MSE A 415:162–170. https://doi.org/10.1016/j.msea.2005.09.032

20. Boyce BL, Reu PL, Robino CV (2006) The constitutive behavior of laser welds in 304L stainless steel determined by digital image correlation. Metall Mater Trans A 37:2481–2492. https://doi.org/10.1007/BF02586221

21. Milosevic M, Milosevic N, Sedmak S, Tatic U, Mitrovic N, Hloch S, Jovicic R (2016) Digital image correlation in analysis of stiffness in local zones of welded joints. Teh vjesn 23(1):19–24. https://doi.org/10.17559/TV-20140123151546

22. Molak RM, Paradowski K, Brynk T, Ciupinski L, Pakiela Z, Kurzydlowski KJ (2009) Measurement of mechanical properties in a 316L stainless steel welded joint. Int J Pres Ves Pip 86:43–47. https://doi.org/10.1016/j.ijpvp.2008.11.002

23. Kartal M, Molak R, Turski M, Gungor S, Fitzpatrick ME, Edwards L (2007) Determination of weld metal mechanical properties utilising novel tensile testing methods. App. Mech Mater 7–8:127–132. https://doi.org/10.4028/www.scientific.net/AMM.7-8.127

24. Ren X, Xu X, Jiang C, Huang Z, He X (2020) Strain distribution and fatigue life estimation for steel plate weld joint low cycle fatigue based on DIC. Opt and Lasers Eng 124:105839. https://doi.org/10.1016/j.optlaseng.2019.105839

25. Langschwager K, Bosch A, Lang E, Rudolph J, Vormwald M, Scholz A, Oechsner M (2014) Fatigue behavior of butt weld seams-experimental investigation and numerical simulation. Proc. ASME Pressure Vessels & Piping Conference 20–24. https://doi.org/10.1115/PVP2014-28787

26. Sriba A, Vogt JB, Amara SE (2018) Microstructure, micro-hardness and impact toughness of welded austenitic stainless steel 316L. Trans Ind Inst Met 71:2303–2314. https://doi.org/10.1007/s12666-018-1362-4

27. Hong SG, Yoon S, Lee SB (2003) The effect of temperature on low-cycle fatigue behavior of prior cold worked 316L stainless steel. Int J Fatigue 25:1293–1300. https://doi.org/10.1016/S0142-1123(03)00154-3

28. Vogt JB, Magnin T, Foct J (1993) Effective stresses and microstructure in cyclically deformed 316L austenitic stainless steel: effect of temperature and nitrogen content. FFEMS 16:555–564. https://doi.org/10.1111/j.1460-2695.1993.tb00766.x

29. Wang B, Hong C, Winther G, Christiansen TL, Somers MAJ (2020) Deformation mechanisms in meta-stable and nitrogen-stabilized austenitic stainless steel during severe surface deformation. Materialia 12:100751. https://doi.org/10.1016/j.mtla.2020.100751

30. Agrawal R, Uddanwadiker R, Padole P (2014) Low cycle fatigue life prediction IJEERT 2:5–15

31. Roya SC, Goyalb S, Sandhyab R, Raya SK (2012) Low cycle fatigue life prediction of 316L(N) stainless steel based on cyclic elasto-plastic response. Nuc Eng Des 253:219–225. https://doi.org/10.1016/j.nucengdes.2012.08.024

32. Facheris G, Pham MS, Janssens KGF, Holdsworth SR (2013) Microscopic analysis of the influence of ratcheting on the evolution of dislocation structures observed in AISI 316L stainless steel during low cycle fatigue. MSE A 587:1–11. https://doi.org/10.1016/j.msea.2013.08.041

33. Phama MS, Solenthaler C, Janssens KGF, Holdsworth SR (2011) Dislocation structure evolution and its effects on cyclic deformation response of AISI 316L stainless steel. MSE A 528(7):3261–3269. https://doi.org/10.1016/j.msea.2011.01.015

34. Obrtlik K, Kruml T, Polak J (1994) Dislocation structures in 316L stainless steel cycled with plastic strain amplitudes over a wide interval. MSE A 187:1–9. https://doi.org/10.1016/0921-5093(94)90325-5

35. Chandra SK, Shankar VN, Mariappan K, Sandhya R, Chakraborty PC (2013) Effect of strain rate on the low cycle fatigue behavior of 316L(N) stainless steel weld joints. Proc Eng 55(3):176–180. https://doi.org/10.1016/j.proeng.2013.03.239

36. Jiang W, Xie X, Wang T, Zhang X, Tu ST, Wang J, Zhao X (2021) Fatigue life prediction of 316L stainless steel weld joint including the role of residual stress and its evolution: experimental and modelling. Int. J. Fatigue. 143:105997. https://doi.org/10.1016/j.ijfatigue.2020.105997

37. Otegui JL, Kerr HW, Burns JJ, Mohaupt HU (1989) Fatigue crack initiation from defects at weld toes in steel. Int J Pres Ves Pip 38:385–417. https://doi.org/10.1016/0308-0161(89)90048-3

38. Schork B, Kucharczyk P, Madia M, Zerbst U, Hensel J, Bernhard J, Tchuindjang D, Kaffenberger M, Oechsner M (2018) The effect of the local and global weld geometry as well as material defects on crack initiation and fatigue strength. Eng Fract Mec 198:103–122. https://doi.org/10.1016/j.engfracmech.2017.07.001

39. Schaumann P, Collmann M (2013) Influence of weld defects on the fatigue resistance of thick steel plates. Pro Eng 66:62–72. https://doi.org/10.1016/j.proeng.2013.12.062

40. Krewerth D, Lippmann T, Weidner A, Biermann H (2016) Influence of non-metallic inclusions on fatigue life in the very high cycle fatigue regime. Int J Fatigue 84:40–52. https://doi.org/10.1016/j.ijfatigue.2015.11.001

41. Prasad Reddy GV, Sandhya R, Valsan M, Bhanu Sankara Rao K (2010) Temperature dependence of low cycle fatigue of 316 (N) weld metals and 316L (N)/ 316 (N) weld joints. Mater Sc Tech 1384-1392. https://doi.org/10.1179/174328408X317110

42. Vogt JB, Salazar D, Proriol Serre I 2013 Partition of cyclic plasticity in the 25Cr-7Ni-0.25N duplex stainless steel investigated by atomic force microscopy. In: Alvarez-Armas I Degallaix-Moreuil S, editors. In Duplex stainless steels, London, pp 275–302. https://doi.org/10.1002/9781118557990.ch8

43. Bultel H, Vogt JB (2010) Influence of heat treatment on fatigue behaviour of 4130 AISI steel. Proc Eng 2:917–924. https://doi.org/10.1016/j.proeng.2010.03.099

44. Giuizani H, Tlili B, Chafra M (2021) Experimental characterization and fatigue behavior of thermally and mechanically treated 316L stainless steel MIG-welded joints. Weld World 65:67–78. https://doi.org/10.1007/s40194-020-00997-x

45. Xu K, Wang X, Cui H, Lu F (2019) Investigation on LCF behavior of welded joint at different temperatures for bainite steel. Chin. J. Mech. Eng. 32:29. https://doi.org/10.1186/s10033-019-0346-6